WIDEBAND VALIDATION OF A PHASE RETRIEVAL PROCESS APPLIED TO INFRARED PLANAR NEAR-FIELD MEASUREMENTS

N. Ribière-Tharaud and M. Lambert

Département de Recherche en Électromagnétisme
Laboratoire des Signaux et Systèmes UMR 8506
(CNRS–SUPELEC-Univ Paris Sud)
3 rue Joliot-Curie, 91190 Gif-sur-Yvette, France

P. Levesque

ONERA DMSC
29 avenue de la Division Leclerc, 92322 Châtillon, France

Abstract—The framework of our work is the application of a fast method to estimate the radiation pattern of an antenna from the measurement of the electric-field magnitude in the near-field region using infrared (IR) camera. IR acquisition techniques allows quasi-realtime measurements of the magnitude of the electrical field on planar surfaces in near-field conditions. However the antennas radiation patterns can only be estimated from near-field electrical magnitude and phase measurements. Consequently a classical plane to plane iterative phase retrieval process has been developed and tested with respect to a large number of configuration parameters such as to find an optimal configuration on a wide frequency range [0.5–20 GHz]. In order to achieve and validate such a study, some comparisons have been performed on data obtained either by numerical simulation or classical near-field technique based upon radio-frequency (RF) probe scanning on simple horn antennas. Among all the studied parameters we will focus onto the influence of the dynamic range of the measurements on the reconstructed radiation patterns and on validations from experimental results.

1. INTRODUCTION

Near-Field (NF) techniques are well suited for the characterization of antennas radiation patterns as long as the radiated field is known in magnitude and phase. However, in a number of configurations of interest, the measurement of the phase is not possible. This issue has become of growing interest considering not only the cost of the measurement equipments and the data acquisition time but also measurement frequencies for which the phase acquisition with a good accuracy is difficult to perform or, as it is with high power microwave (HPM) sources, when the intensity of the electric field to be measured is too high. Another configuration matching to this condition is occurring when the measurement setup is dedicated specifically to magnitude measurements of the radiated fields as the one presented in the following.

   Many phase retrieval techniques using magnitude only measurements have been developed for various application areas [3, 4, 6, 7, 9, 10, 13–17, 20]. In most cases, the known of the source geometry is used in combination with an optimization procedure. The classical technique is an iterative plane-to-plane (PTP) process sometimes combined with complementary optimization approach such as genetic algorithm or particle swarm optimization in order to find a better initial guess [16]. The PTP technique implies the knowledge of the magnitude of the radiated field on two separated planes to ensure the diversity of the data. Nevertheless, the measurements can be achieved twice in the same plane if the diversity is obtained by changing the propagation media properties between the two sets of measurements [20]. A direct process is proposed in [10] using the magnitude known on one or more arbitrary surfaces and a gradient optimization scheme to derive equivalent sources on the antenna aperture. Comparisons of some of these approaches are also proposed in [4, 7, 16].

   The results presented in this paper are based upon the classical iterative PTP phase retrieval process [5, 6, 14, 15] as far as no a-priori information related to the source geometry is available and because of the huge number of unknowns involved. To optimize the measurement configuration a parametric study has been performed on the distance between the acquisition planes and their sizes and also on the number of acquisition points per wavelength. This approach has been validated for antenna characterization on a wide frequency range [0.5–20 GHz] using data obtained from near-field measurements.

   The considered infrared measurement setup shows some drawbacks that can affect the phase reconstruction algorithm presented. In particular, the dynamic range of the data appears to be a key parame-

ter to have a good phase reconstruction and thus for relevant far-field evaluation. We will then focus on that aspect and present some numerical and experimental results to evaluate the minimal dynamic range needed for this kind of algorithm. This paper differs from [14] and [15] since a full parametric study is carried out and wide band application is considered.

Note that in the following only single polarized antenna will be considered. However the case of dual polarized antenna has been recently addressed in the literature [4, 18].

2. THE IR MAPPING TECHNIQUE

The EMIR© measurement technique is an infrared thermographic imaging method based upon the use of a thin photothermal film which is able to convert a part of the total incident electric field into heat [1, 11]. The heating is then detected using an infrared camera working between 5 and 1500 Hz. Fig. 1 shows a typical test setup for antenna characterization.

Such a technique allows to achieve a complete evaluation of the electric field magnitude on one planar surface in a few seconds which is much faster than classical RF probe scanning. Moreover, it is a non invasive technique (see [1, 11] for the details of such photothermal tool for the electromagnetic phenomena characterization) and several measurement plane positions can be assessed very rapidly by changing
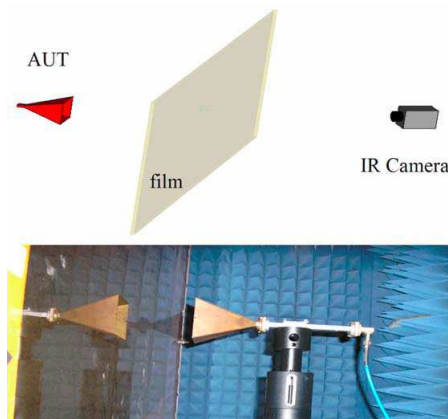
Figure 1. Classical test setup for antenna measurement using EMIR© (top). Photo of the antenna under test (AUT) and the photothermal film (bottom).

the distance AUT-film. However, some drawbacks are inherent to the technique. Thus we have to consider the extents of the film that can limit the ability to reconstruct the far-field pattern. For instance, the camera resolution is 320×240 pixels leading to measurement plane of maximum size equal to $1.6 \times 1.2\,\text{m}^2$ with a $\lambda/3$ discretization step at $f = 20\,\text{GHz}$. The dynamic of the measurement is also a critical point [15]. In order to improve the latter, an averaging on several images is applied (typically 8000 images are captured). A thermal convection occurs during the acquisition and is taken into account by the use of an amplitude modulation of the source combined to a coherent detection process.

In order to illustrate the efficiency of the method, the field radiated by a standard horn antenna has been simulated using a commercial software (FEKO$^©$) and measured using the EMIR$^©$ technique and a classical RF probe scanning one at $8\,\text{GHz}$. A comparison of the normalized electric fields for the two main cuts in a plane located at 2λ from the antenna aperture is presented in Fig. 6. The results show a good agreement, the main difference being linked to the dynamic range of the measurements limited to $30\,\text{dB}$ in the case of the EMIR$^©$ method in this specific configuration.

3. THE PHASE RETRIEVAL PROCESS

The phase reconstruction is achieved assuming that the electric field distribution is known in magnitude on two planes parallels to the antenna aperture and located at distances x_1 and x_2 from it. The antenna position is described using a Cartesian coordinate system, such that x_i is the position on a x-axis orthogonal to the AUT aperture, the origin being at the center of the aperture.

3.1. Description of the Phase Reconstruction Algorithm

In this iterative approach, each iteration $\#k$ can be described in four steps (Fig. 2).

- Let us defined the complex-valued electric field $\tilde{E}_1^k(x_1, y, z)$ onto the plane P_1 at position x_1 by

$$\tilde{E}_1^k(x_1, y, z) = |\xi_1(x_1, y, z)|\, \text{e}^{j\phi_1^k(x_1,y,z)} \qquad (1)$$

where $|\xi_1(x_1, y, z)|$ denotes the measured field magnitude on the plane P_1, (x_1, y, z) a position in the plane P_1 and $\phi_1^k(x_1, y, z)$ a known phase obtained from the previous iteration (at iteration $\#1$, $\phi_1^0(x_1, y, z)$ is initialized to zero all over the plane).
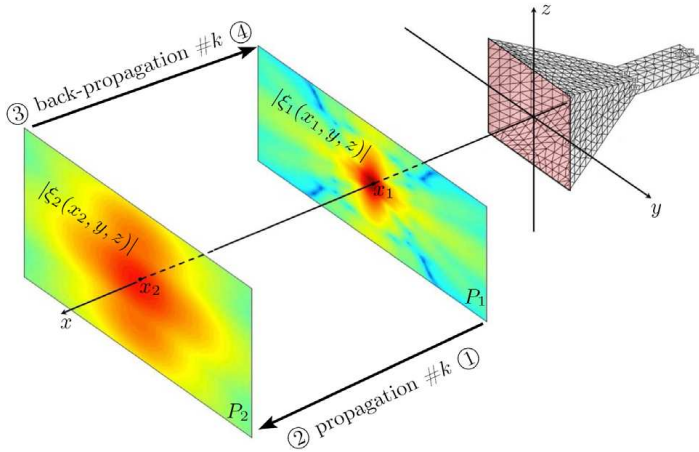
Figure 2. The four steps of the phase retrieval process considering the kth iteration.

- $\tilde{E}_1^k(x_1, y, z)$ is then propagated from P_1 to P_2 using the plane wave spectrum decomposition to get the complex-valued electric field $\tilde{E}_2^k(x_2, y, z)$ given by (2).

$$\tilde{E}_2^k(x_2, y, z) = \left| E_2^k(x_2, y, z) \right| \mathrm{e}^{j\phi_2^k(x_2, y, z)} \qquad (2)$$

  The computed magnitude $\left| E_2^k(x_2, y, z) \right|$ is different from the measured field $|\xi_2(x_2, y, z)|$ since the phase $\phi_1^k(x_1, y, z)$ used to compute the propagation is not the exact one.

- The computed magnitude $\left| E_2^k(x_2, y, z) \right|$ is replaced by the measured one $|\xi_2(x_2, y, z)|$ leading to (3).

$$\tilde{E}_2^k(x_2, y, z) = |\xi_2(x_2, y, z)| \mathrm{e}^{j\phi_2^k(x_2, y, z)} \qquad (3)$$

- The field $\tilde{E}_2^k(x_2, y, z)$ is then back-propagated to the plane P_1 at the position x_1 and is given by (4)

$$\tilde{E}_1^k(x_1, y, z) = |E_1^k(x_1, y, z)| \mathrm{e}^{j\phi_1^k(x_1, y, z)} \qquad (4)$$

  The computed magnitude $\left| E_1^k(x_1, y, z) \right|$ is different from the measured field $|\xi_1(x_1, y, z)|$ since the phase $\phi_2^k(x_2, y, z)$ used to compute the propagation is not the exact one. The computed magnitude $\left| E_1^k(x_1, y, z) \right|$ is replaced by the measured one $|\xi_1(x_1, y, z)|$ leading to (1) with $k = k + 1$.

  The reconstruction algorithm is stopped at iteration k when the computed field magnitudes $\left| E_1^k(x_1, y, z) \right|$ and $\left| E_2^k(x_2, y, z) \right|$ are close

enough to the measured ones $|\xi_1(x_1, y, z)|$ and $|\xi_2(x_2, y, z)|$, is to say for a low cost function Δ_n^k given by

$$\Delta_n^k = \frac{\displaystyle\sum_{i=1}^{N_y} \sum_{j=1}^{N_z} \left| \left\| E_n^k(x_n, y_i, z_j) \right\| - \left\| \xi_n(x_n, y_i, z_j) \right\| \right|^2}{\displaystyle\sum_{i=1}^{N_y} \sum_{j=1}^{N_z} \left\| \xi_n(x_n, y_i, z_j) \right\|^2}. \tag{5}$$

The convergence and the uniqueness of phase retrieval algorithms have been constantly studied and only a brief statement of the problem and the corresponding references will be given. As explained in [3] for the case of the far-field pattern determination from near-field amplitudes or in [2] for a more general overview in the optical domain, such a kind of algorithms can be seen as alternating projection algorithms. In [2] (and the hundred references herein) the authors propose a link between the classical phase retrieval algorithms and their counterpart in the classical convex optimization methods whereas in [12] an unified notation of the different approaches is proposed. The adopted reconstruction scheme is known to have a local convergence and then to be very sensitive to the initialisation of the phase.

3.2. The Parameters of the Phase Retrieval Process

Once the reconstructed complex field made of the measured near-field combined to the reconstructed phase has been obtained, the corresponding far-field is computed using a classical near-field to far-field transformation [21]. As far as the far-field of the AUT is the main goal, the quality of the phase reconstruction is measured by comparing the magnitude of the reconstructed far-field E_{FF} to the reference one ξ_{FF} using (6). The phase is ignored in the error evaluation since the reconstructed phase distribution is unique up to a constant [8].

$$\Delta_{\text{FF}} = \frac{\displaystyle\sum_{i=1}^{N_\theta} \sum_{j=1}^{N_\varphi} \left| \left\| E_{\text{FF}}(\theta_i, \varphi_j) \right\| - \left\| \xi_{\text{FF}}(\theta_i, \varphi_j) \right\| \right|^2}{\displaystyle\sum_{i=1}^{N_\theta} \sum_{j=1}^{N_\varphi} \left\| \xi_{\text{FF}}(\theta_i, \varphi_j) \right\|^2} \tag{6}$$

Several parameters are of importance in the reconstruction process. Among all of them the positions of the two planes, their sizes and the discretization of the planes have been extensively studied in [19] and validated on numerical and experimental data over the frequency band of interest. Results show that the good configuration is given for $x_1 = 2\lambda$ and $x_2 = 3\lambda$ with a discretization step equal or lower than
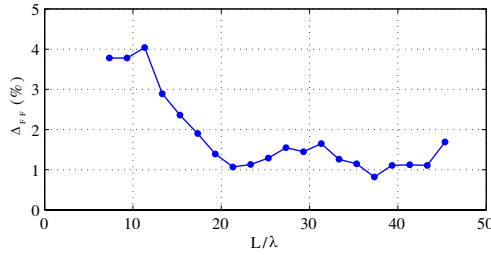
Figure 3. $f = 8\,\mathrm{GHz}$. Variation of the errors on reconstructed far-fields Δ_{FF} (in %) with respect to the planes sizes L expressed as a number of wavelength λ.

$\lambda/3$ and a size L greater than 20λ. As an illustration the evolution of Δ_{FF} with respect to the size of the plane L is presented in Fig. 3.

## 4. ASSESSMENTS ON THE DYNAMIC RANGE

4.1. Introduction

In the following a special attention is dedicated to the influence of the dynamic range of the measurements onto the retrieval process. The radiating source is a horn antenna working at $8\,\mathrm{GHz}$ frequency. It has been simulated using a MoM method allowing the computation of the reference far-field and of the radiated near-field on several planes. In order to assess the dynamic range, a Gaussian random noise has been added to the computed exact data. The noise distribution is defined by a zero mean and by a variance σ which is representing the mean power associated to the noise. The noise level is then characterized using the definition of the signal to noise ratio (SNR_i).

$$\mathrm{SNR}_i = 10 \log \left[\frac{\max \left(\|\xi_i\|^2 \right)}{\sigma^2} \right] \qquad (7)$$

where $\max \left(\|\xi_i\|^2 \right)$ is the maximum of the square of the measured magnitude on the plane i. Furthermore, the specific IR measurement configuration is taken into account by applying an averaging process of 100 realizations of random noise applied to the exact data leading to the final noisy data. Six levels of noise between $12\,\mathrm{dB}$ and $70\,\mathrm{dB}$ have been studied (Fig. 4).

4.2. Validation of the Noise Representation

The noise scheme is validated by comparison of the reconstructed radiation patterns using either IR measurements or synthetic $32.63\,\mathrm{dB}$
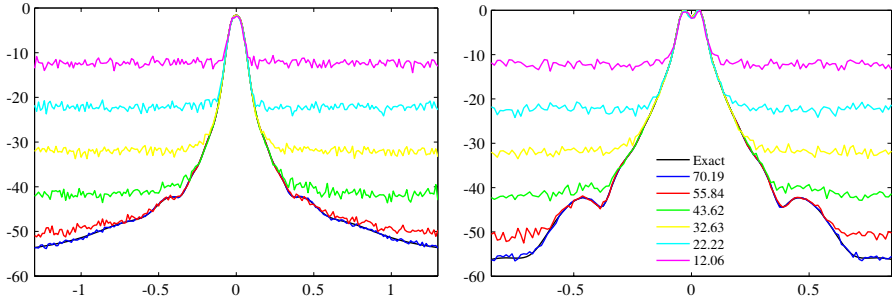
Figure 4. $f = 8\,\text{GHz}$. Effect onto the exact synthetic data of our noise model for different level on a plane located at 2λ from the source aperture. Averaging on 100 realizations is carried out. Vertical cut (left) and horizontal cut (right).

noise level data. A comparison of the maps of the electric field magnitude (in dB) measured on a plane at 2λ are presented in Fig. 5 for the noiseless synthetic case (Fig. 5(a)), the 32 dB-noise level (Fig. 5(c)), the RF (Fig. 5(b)) and IR measurements (Fig. 5(d)). As expected the highest intensity regions (at the center of the map) are very similar in all the cases whereas the lowest intensity ones for 32 dB-noise level numerical simulation and for IR measurements show the same behavior. A comparison of the two main cuts of the four corresponding data are shown in Fig. 6 and confirm the similarity of the curves.

4.3. Effect of the Dynamic Range

Phase reconstructions have been carried out for the six noise configurations described in Section 4.1. The evolution of the error Δ_{FF} with respect to the noise level is presented Fig. 7 for two cases: with the raw near-field data and with the filtered ones. As a matter of fact using the raw data leads to a very oscillating solution due to the Gibbs phenomena related to the combination of the discontinuity of the measurements and the use of the FFT. The lower the noise level is the higher the oscillations are and the higher Δ_{FF} is. As an illustration a comparison between the filtered and raw near-field data at 32.63 dB is proposed in Fig. 6 and the corresponding reconstructed far field in Fig. 8.

To overcome such a problem a filtering algorithm based on a noise level threshold have been applied. All the values lower than the chosen threshold are set to zero. Applying the reconstruction process onto such filtered data allows to significantly reduce the errors as exemplified in Fig. 7.
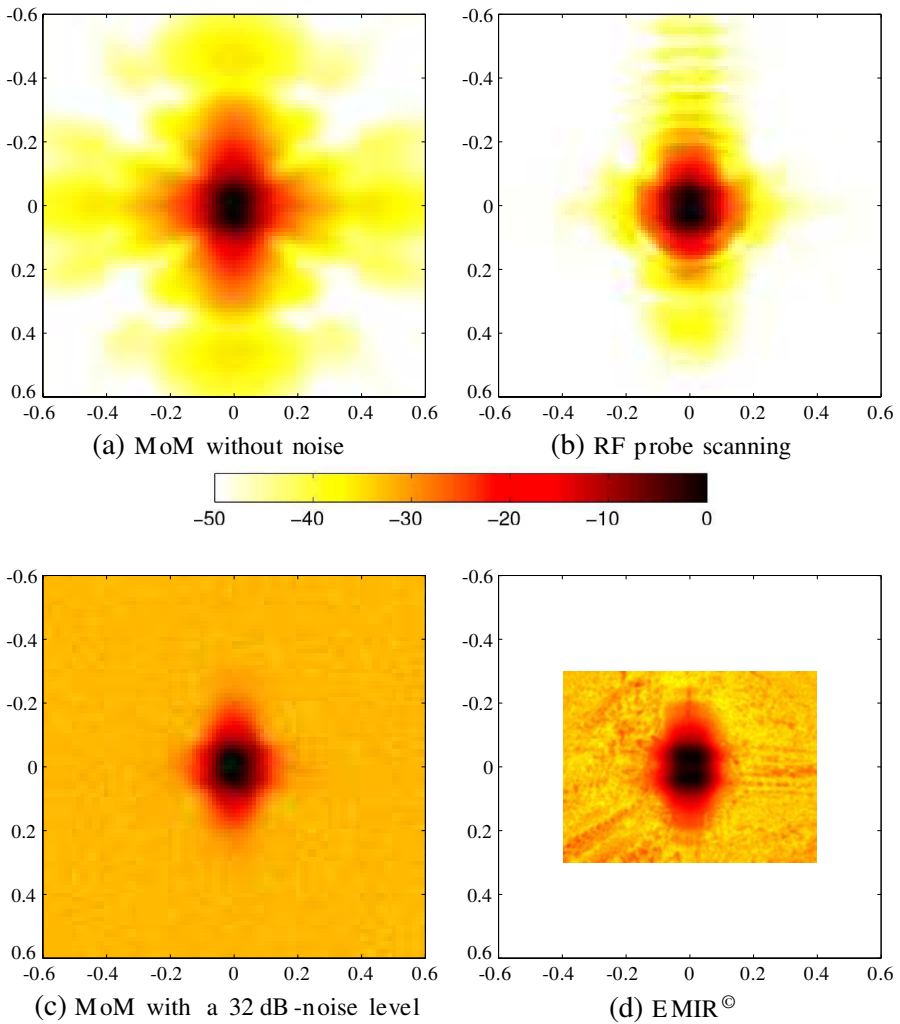
Figure 5. $f = 8\,\text{GHz}$. Colormap of the normalized electric fields simulated (a) without noise and (c) with a $32\,\text{dB}$-noise level, measured (b) with a RF probe or (d) with EMIR$^{©}$ method on a plane at 2λ from the AUT aperture.

In Fig. 8 are compared the far-field reconstructions obtained by our process from the filtered numerical noisy data presented in Fig. 4. As illustrated by the evolution of Δ_{FF} with respect to the SNR level (Fig. 7) the higher the latter is the worst the far-field is. However, up to a SNR of $32\,\text{dB}$ the result is still acceptable and it can be seen as a SNR limit for which our process is efficient.
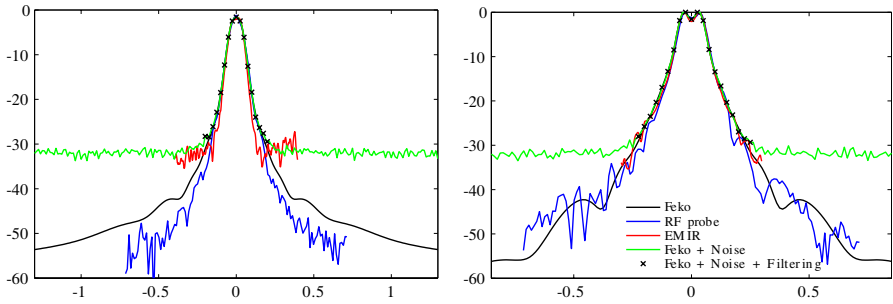
Figure 6. $f = 8\,\text{GHz}$. Comparison of the normalized electric fields simulated without noise (black), with a $32\,\text{dB}$-noise level without filtering (green) and with (cyan), measured with a RF probe (dark blue) or with EMIR$^{©}$ method (red) on a plane at 2λ from the AUT aperture. Vertical cut (left) and horizontal cut (right).
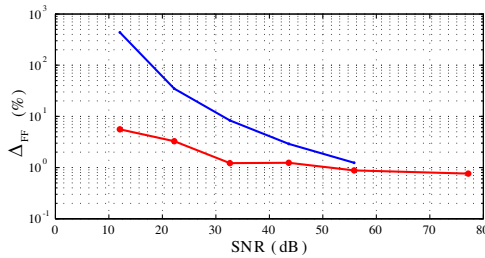
Figure 7. $f = 8\text{GHz}$. Effect of noise added to the computed electric field on the reconstructed far-field, without (blue dots) and with (red stars) filtering the near-field data.
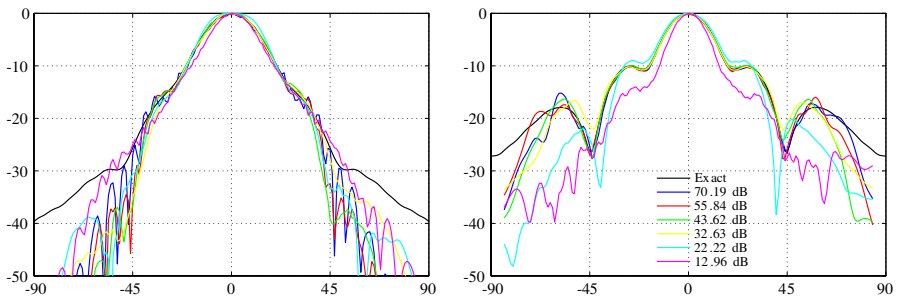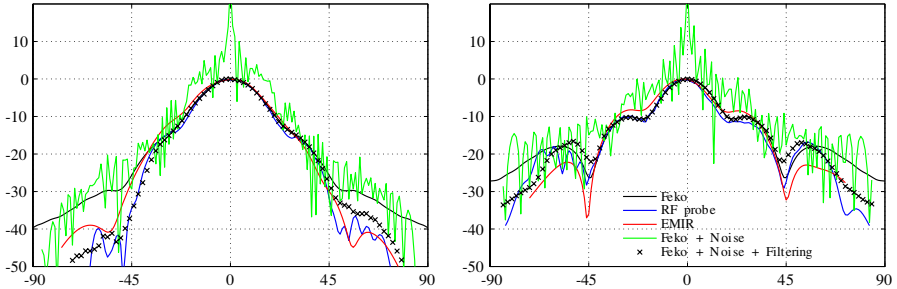

Figure 8. $f = 8\,\text{GHz}$, horizontal (left) and vertical (right) cut of the normalized far-fields obtained by our process using the numerical noisy data presented Fig. 4.
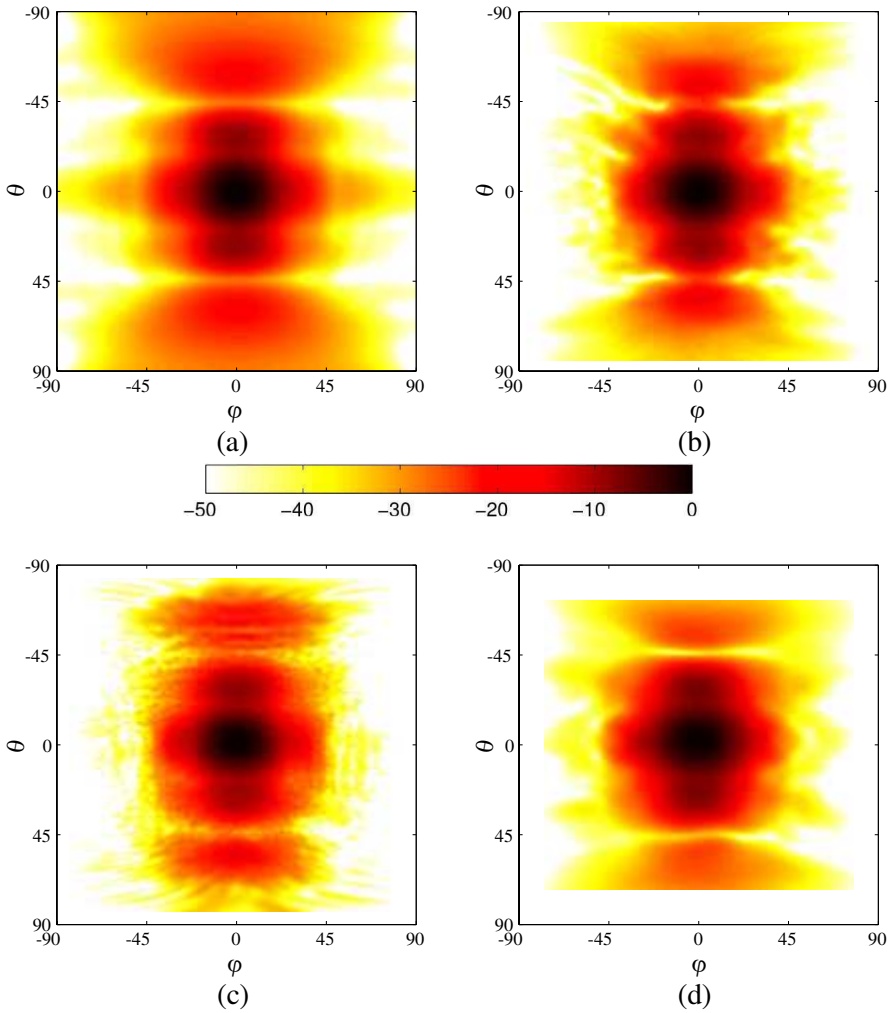
Figure 9. $f = 8\,\text{GHz}$, normalized far-fields $|F_\theta(\theta, \varphi)|$ in dB; (a) MoM-reference, (b) reconstructed from noisy numerical data, (c) reconstructed from RF probe measurements and (d) IR measurements.

The efficiency of the reconstruction process is illustrated by comparing (Fig. 9) a map of the "exact" normalized far-field $|F_\theta(\theta, \varphi)|$ at $f = 8\,\text{GHz}$ with the ones obtained via our reconstruction process either by using simulated data with a $32.63\,\text{dB}$ SNR with filtering (the one without filtering is not presented) or IR measurement data. In Fig. 10 are compared the two cuts — vertical ($\varphi = 0°$) and

Figure 10. $f = 8\,\text{GHz}$, horizontal (left) and vertical (right) cut of the normalized far-fields presented in Fig. 9: reference (MoM) (black), reconstructed from noisy numerical data with filtering (x) and without (green) reconstructed from RF probe measurements (dark blue) and IR measurements (red).

horizontal $(\theta = 0°)$ — of the normalized far-field showing a good agreement between reconstructions obtained from simulated data and from experimental which validates thus our noise representation. In order to illustrate the effectiveness of the filtering the normalized far-field obtained from non-filtered data has been added. As previously explained, the use of raw data leads to a non acceptable oscillating solution whereas the filtered noisy data and the measured data (RF and IR) well fit the theoretical solution. Moreover, the good agreement between reconstructions from filtered simulated data with a SNR of 32 dB and from IR experiments validates the chosen noise representation.

5. EXPERIMENTAL VALIDATION ON A WIDE FREQUENCY RANGE

In order to validate the reconstruction method on a wide frequency range our process has been applied onto IR measurements obtained at other frequencies. For lake of place only two (3.8 GHz and 18 GHz) are presented here. For those frequencies the acquisition configuration met the previous requirements for the dynamic range but not for the size of the acquisition planes at low frequency (Table 1), the latter being due to the limited size of the photothermal film we had at that time.

For those frequencies the reconstructed far-fields obtained from IR measurements are compared to the measured far-fields provided by the CEG (Centre d'Étude de Gramat) from the CEA-DAM (Commissariat

Table 1. IR measurements parameters.

Frequency (GHz)	Planes size (m)	NF dynamic range (dB)
3.8	$19.75\lambda \times 14.73\lambda$	33
18	$61.41\lambda \times 38.86\lambda$	40
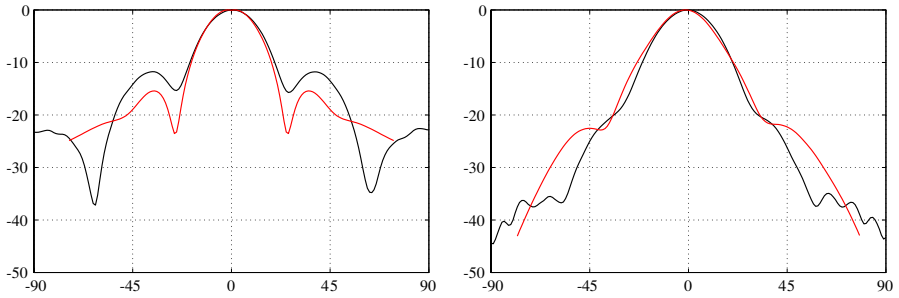
Figure 11. $f = 3.8\,\text{GHz}$, normalized far-fields, bottom $F_\theta(\theta, \varphi = 0°)$ and top $F_\theta(\theta = 0°, \varphi)$, measured reference (black), reconstructed from IR measurements (red).
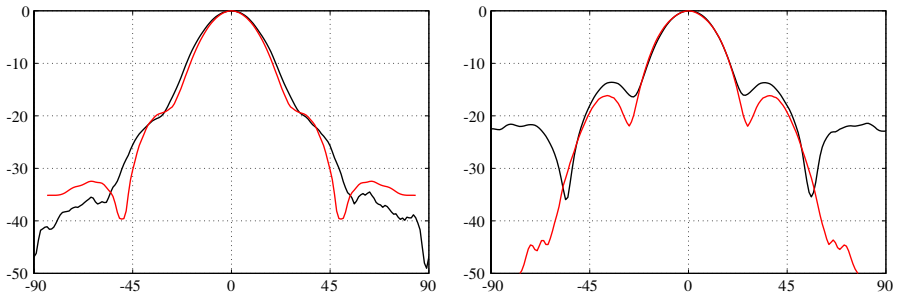
Figure 12. $f = 18\,\text{GHz}$, normalized far-fields, bottom $F_\theta(\theta, \varphi = 0°)$ and top $F_\theta(\theta = 0°, \varphi)$, measured reference (black), reconstructed from IR measurements (red).

à l'Énergie Atomique-Direction des Applications Militaires[†]). A good agreement between reference and reconstructed far-fields can be observed (Fig. 11 and Fig. 12).

[†] Military Applications Division

6. CONCLUSION

A phase retrieval process has been assessed on numerical data and validated on IR experimental data focusing on the dynamic range of the data. A dynamic range of 30 dB has to be reached on the near-field measurements to ensure a good reconstruction of the phase and thus a good far-field estimation. Furthermore, it has been shown that the method efficiency is increased if a threshold is applied to the measurements in order to keep only the useful part of the signal. The validation has been carried out on a wide frequency range and shows that IR techniques, and more particularly the EMIR$^©$ method, can be used for fast measurement of antennas radiation patterns in near-field conditions. Future work includes the extension of this parametric study to bi-polarized near-field data, involving the use of anisotropic photo thermal films.

ACKNOWLEDGMENT

REFERENCES

1. Balageas, D. and P. Levesque, "EMIR: A photothermal tool for electromagnetic phenomena characterization," *Revue Générale de Thermique*, Vol. 37, 725–739, 1998.

2. Bauschke, H. H., P. L. Combettes, and D. R. Luke, "Phase retrieval, error reduction algorithm, and fienup variants: A view from convex optimization," *Journal of Optical Society of America*, Vol. 19, 1334–1345, 2002.

3. Bucci, O. M., G. D'elia, G. Leone, and R. Pierri, "Far-field pattern determination from the near-field amplitude on two surfaces," *IEEE Transactions on Antennas and Propagation*, Vol. 38, No. 11, 1772–1779, 1990.

4. Capozzoli, A., C. Curcio, G. D'Elia, and A. Liseno, "Phaseless antenna characterization by effective aperture field and data representations," *IEEE Transactions on Antennas and Propagation*, Vol. 57, 215–230, 2009.

[‡] Two of the authors would like to dedicate this paper to the memory of the latter who suddenly passed away in February 2010.

5. Gonzalez-Arbesu, J., S. Blanch, A. Aguasca, and J. Romeu, "Fast far-field antenna pattern determination using infrared thermograms and phase retrieval algorith," *IEEE Antennas and Propagation Society International Symposium*, 710–713, 2002.

6. Gonzalez-Arbesu, J. M., "Caracterization de antenas mediante termographias de infrarrojos," Ph.D. thesis, Universidad Politecnica de Cataluna, 2000.

7. Hislop, G., G. C. James, and A. Hellicar, "Phase retrieval of scattered fields," *IEEE Transactions on Antennas and Propagation*, Vol. 55, 2332–2341, 2007.

8. Hoenders, B. J., "On the solution of the phase retrieval problem," *Journal of Mathematical Physics*, Vol. 16, 1719–1725, 1975.

9. Isernia, T., G. Leone, and R. Pierri, "Radiation pattern evaluation from near-field intensities on planes," *IEEE Transactions on Antennas and Propagation*, Vol. 44, 701–710, 1996.

10. Las-Heras, F. and T. K. Sarkar, "A direct optimization approach for source reconstruction and NF-FF transformation using amplitude-only data," *IEEE Transactions on Antennas and Propagation*, Vol. 50, 500–510, 2002.

11. Levesque, P., L. Leylekian, A. Déom, and D. Balageas, "Latest developments in the EMIR technique of infrared imaging electromagnetic fields," *Society of Photo-optical Instrumentation Engineers (SPIE) Conference Series*, A. E. Rozlosnik and R. B. Dinwiddie (eds.), Vol. 4360, 48–59, 2001.

12. Marchesini, S., "Invited article: A unified evaluation of iterative projection algorithms for phase retrieval," *Review of Scientific Instruments*, Vol. 78, 011301, 2007.

13. Migliore, M. D., F. Soldovieri, and R. Pierri, "Far-field antenna pattern estimation from near-field data using a low-cost amplitude-only measurement setup," *IEEE Transactions on Instrumentation and Measurement*, Vol. 49, 71–76, 2000.

14. Norgard, J., "Electromagnetic magnitude and phase measurements from infrared thermograms," *IEEE Proceedings Aerospace Conference*, Vol. 2, 145–157, 1997.

15. Norgard, J., J. Will, and C. Stubenrauch, "Quantitative images of antenna patterns using infrared thermography and microwave holography," *International Journal of Imaging Systems and Technology*, Vol. 11, 210–218, 2000.

16. Puskely, J. and Z. Novácek, "Application of the global optimization approaches to planar near-field antenna phaseless measurements," *Radioengineering*, Vol. 18, 9–17, 2009.

17. Razavi, S. F. and Y. Rahmat-Samii, "A new look at phaseless planar near-field measurements: Limitations, simulations, measurements, and a hybrid solution," *IEEE Antennas and Propagation Magazine*, Vol. 49, 170–178, 2007.

18. Razavi, S.-F. and Y. Rahmat-Samii, "Polarization extraction in planar near-field phaseless measurements," *IEEE Transactions on Antennas and Propagation*, Vol. 56, 3233–3240, 2008.

19. Ribière-Tharaud, N., A. Casagranda, M. Lambert, and F. Jouvie, "Numerical and experimental assessment of a phase retrieval technique applied to planar near-field distribution for wide band applications," *3th International Conference on Near-field Characterization and Imaging (ICONIC'07)*, 194–199, SaintLouis, USA, 2007.

20. Soldovieri, F., G. Leone, and R. Pierri, "An innovative phase retrieval technique from single-plane near-field intensity by a dielectric slab," *AEU — International Journal of Electronics and Communications*, Vol. 62, 732–739, 2008.

21. Yaghjian, A. D., "An overview of near-field antenna measurements," *IEEE Transactions on Antennas and Propagation*, Vol. 34, 30–45, 1986.